DEVELOPMENT OF AN INVERSE MODULE AND OF A SEMI-ANALYTICAL SENSITIVITY ANALYSIS FOR THERMO-MECHANICAL PARAMETER IDENTIFICATION

Romain FORESTIER, Yvan CHASTEL, Elisabeth MASSONI

CEMEF, Ecole Nationale Supérieure des Mines de Paris, BP 207, 06904 Sophia Antipolis Cedex, France.

Emails : Romain.Forestier@ensmp.fr, Yvan.Chastel@ensmp.fr, Elisabeth.Massoni@ensmp.fr

ABSTRACT :

Numerical simulations of forming processes require a good knowledge of the constitutive parameters of the material. These parameters are identified using laboratory tests which reproduce the conditions of forming processes. If mechanical tests involve large strain, the material flow within the sample may not be homogeneous and the use of an inverse model may be necessary.

The present paper describes an inverse method coupled with a finite element software. The direct model solves a strongly coupled thermo-mechanical equilibrium problem using an incremental approach. Since the discrete system is non–linear, it is solved using an iterative procedure based on a Newton-Raphson algorithm. State variables are updated using a Lagrangian formulation and automatic remeshing algorithm is used to avoid element degeneracy.

The inverse problem is presented as the minimisation of a least square function and is solved using a stabilised Gauss-Newton algorithm. The sensitivity analysis is obtain by using a semi-analytical method, which permits to identify various model. Furthermore, this method is compatible with the remeshing algorithm as opposed to the classical finite difference scheme.

When the number of parameters to identify is relatively important, the Gauss-Newton method may become unstable due to correlation effects between the parameters. It is shown that for the identification of complex constitutive law parameters, the inverse problem becomes ill-

conditioned. A stability analysis is presented in order to understand the reasons of the unstability and a stabilisation method is proposed.

KEYWORDS :

Inverse problem, semi-analytical sensitivity analysis, stability analysis, constitutive law, friction law

NOMENCLATURE :

$\dot{\varepsilon}^p$	plastic strain rate tensor
$\dot{\varepsilon}^e$	elastic strain rate tensor
$\dot{\varepsilon}$	total strain rate tensor
σ	Cauchy stress tensor
s	deviatoric part of the stress tensor
p	hydrostatic pressure ,
v	velocity of the material,
P	discrete hydrostatic pressure ,
V	discrete velocity of the material,
v_{die}	velocity of the die,
n	outside normal of the piece,
Ω	domain of the piece
$\partial\Omega_f$	free surface
$\partial\Omega_c$	contact surface with the dies
$\dot{\bar{\varepsilon}}$	equivalent plastic strain rate
$\bar{\varepsilon}$	equivalent plastic strain
C^e	elasticity tensor
σ_0	flow stress
λ^c	vector containing the set of constitutive parameters to be identified
λ^f	vector containing the set of friction parameters to be identified
λ	vector containing the parameters to be identified
T	temperature of the material
T_p	temperature of the part on the free edge

T_{ext}	external temperature
T_{int}	interface temperature between the part and the die
k	thermal conductivity
ρc	heat capacity
ρ	penalty coefficient
d	admissible penetration distance
Δt	time discretisation step
$\Delta\lambda$	finite difference step
X	mesh coordinates
$F(\lambda)$	vector containing computed data from the direct model
M	vector containing experimental data
λ^{opt}	optimal set of parameters
W	weight matrix
ϕ	cost function

1 INTRODUCTION

Numerical simulations of forming processes require an accurate knowledge of material properties. Therefore, constitutive parameter identification is a necessary step in order to perform realistic simulations. In general, simple mechanical tests are used and analysed using analytical models. But, in order to simulate forming processes, it is necessary to study mechanical tests involving high strains. Moreover, the strain paths involved in the forming process and in the associated mechanical tests have to be similar. These constraints imply that inhomogeneous strain fields are often encountered during large strain mechanical tests. Then, constitutive parameter identification may be complicated since it is generally impossible to use a realistic analytical model to analyse such tests.

Gavrus et al. [1] have developed an inverse model coupled to a FEM software to identify constitutive parameters using torsion tests. Massoni et al. [2] use a similar inverse method to identify constitutive and friction parameters from compression tests. One can also cite Mahnken and Stein [3] who identify constitutive parameters from inhomogeneous traction tests. All these studies have be done to analyse 2D transient mechanical tests. In this paper, an inverse analysis coupled to a 3D FEM software is described. The direct model is a software devoted to the thermo-mechanical simulation of forming processes. The formulations chosen

to solve the mechanical and the thermal problem are described in the first section of the paper. Afterwards, the inverse problem is presented as an optimisation problem solved by the Gauss-Newton algorithm. A stabilisation method is proposed in order to avoid instabilities which may develop due to correlation effects between the parameters to be identified, and the sensitivity analysis is done using a semi-analytical scheme [4]. The last section of this work deals with the analysis of plain strain compression tests and of elliptic bulging tests.

2 DIRECT MODEL

2.1 CONSERVATION EQUATIONS AND LIMIT CONDITIONS

The software FORGE3® has been used in order to simulate the mechanical tests. This software is devoted to the thermo-mechanical simulation of the forming processes. The material flow of a domain $\Omega(t)$ at time t is described by the plastic incompressibility (1), the mechanical equilibrium (2) and the heat equation (3) :

$$\mathrm{div}(v) = \mathrm{trace}(\dot{\varepsilon}^e) \qquad \text{in } \Omega(t) \tag{1}$$

$$\mathrm{div}(\sigma) = 0 \qquad \text{in } \Omega(t) \tag{2}$$

$$\rho c_p \frac{dT}{dt} - \nabla.(k\nabla T) = \sigma : \dot{\varepsilon} \qquad \text{in } \Omega(t) \tag{3}$$

$$\dot{\varepsilon} = \frac{\nabla v + \nabla v^T}{2} \qquad \dot{\varepsilon} = \dot{\varepsilon}^e + \dot{\varepsilon}^p \tag{4}$$

where v is the velocity, σ is the stress tensor, T is the temperature, ρc_p is the heat capacity, k the heat conductivity, $\dot{\varepsilon}$ the strain rate tensor, $\dot{\varepsilon}^e$ the elastic strain rate tensor and $\dot{\varepsilon}^p$ the plastic strain rate tensor. Three kinds of boundary conditions may be taken into account to solve the mechanical problem :

Free surface condition :

$$\sigma n = 0 \ \text{ on } \partial\Omega_1(t) \tag{5}$$

Imposed pressure :

$$\sigma n = -P_{imp} n \qquad \text{on } \partial\Omega_p(t) \tag{6}$$

Unilateral contact and friction law :

$$\left.\begin{array}{l}(v - v_{out}).n \le 0 \\ \sigma_n \le 0 \\ \sigma_n (v - v_{out}).n = 0\end{array}\right\} \quad \text{on } \partial\Omega_c(t) \text{ (unilateral contact)} \tag{7}$$

$$\sigma_t = \tau(\Delta v_t) \quad \text{on } \partial\Omega_c(t) \text{ (friction law)} \tag{8}$$

Two boundary conditions are considered for the thermal problem :

Dirichlet condition :

$$T = T_D \quad \text{on } \partial\Omega_D(t) \tag{9}$$

Neumann condition :

$$-k\nabla T.n = \Phi_N \quad \text{on } \partial\Omega_N(t) \tag{10}$$

In order to obtain a well-posed problem and to complete the set of conservation equations, one has to introduce a constitutive law and a friction law.

2.2 CONSTITUTIVE EQUATIONS

If the material behaviour is isotropic, the Von Mises plastic yield criterion is considered

$$\begin{array}{l} f(\sigma, \bar{\varepsilon}, \dot{\bar{\varepsilon}}, T) \le 0 \\ \text{with} \quad f(\sigma, \bar{\varepsilon}, \dot{\bar{\varepsilon}}, T) = \bar{\sigma} - \sigma_0(\bar{\varepsilon}, \dot{\bar{\varepsilon}}, T) \end{array} \tag{11}$$

$$\begin{array}{l} \bar{\sigma}^2 = \dfrac{3}{2} s : s \qquad \dot{\bar{\varepsilon}}^2 = \dfrac{2}{3} \dot{\varepsilon}^p : \dot{\varepsilon}^p \\ s = \sigma + p\,I \qquad \dfrac{d\bar{\varepsilon}}{dt} = \dot{\bar{\varepsilon}} \qquad p = -\dfrac{1}{3}\text{trace}(\sigma) \end{array} \tag{12}$$

where σ_0 is the flow stress, $\bar{\sigma}$ the equivalent stress, s the deviatoric part of the stress tensor, p the hydrostatic pressure, T the temperature, $\bar{\varepsilon}$ the equivalent strain, $\dot{\bar{\varepsilon}}$ the equivalent strain rate and and $\dot{\varepsilon}$ the strain rate tensor. If the material behaviour is anisotropic, the Hill 1948 yield criterion [5] is used :

$$\begin{array}{l} f_H(\sigma, \bar{\varepsilon}, \dot{\bar{\varepsilon}}, T) \le 0 \\ \text{with} \quad f_H(\sigma, \bar{\varepsilon}, \dot{\bar{\varepsilon}}, T) = \bar{\sigma}_H - \sigma_0(\bar{\varepsilon}, \dot{\bar{\varepsilon}}, T) \end{array} \tag{13}$$

$$\bar{\sigma}_H{}^2 = F(\sigma_{22} - \sigma_{33})^2 + G(\sigma_{33} - \sigma_{11})^2 + H(\sigma_{11} - \sigma_{22})^2 + 2L\sigma_{23}^2 + 2M\sigma_{13}^2 + 2N\sigma_{12}^2 \tag{14}$$

where F, G, H, L, M and N are the anisotropic coefficients. The flow stress may be given by various constitutive models :

(model 1) power law : $$\sigma_0 = \mathrm{K}\bar{\varepsilon}^{\mathrm{n}} \tag{15}$$

(model 2) $$\begin{cases} \sigma_0 = \sqrt{3}\left[(1-\mathrm{W})\mathrm{K}_0 \exp\left(\dfrac{\beta}{\mathrm{T}}\right)(\bar{\varepsilon})^{\mathrm{n}} + \mathrm{W}\mathrm{K}_{\mathrm{sat}} \exp\left(\dfrac{\beta_{\mathrm{sat}}}{\mathrm{T}}\right)\right]\left(\sqrt{3}\dot{\bar{\varepsilon}}\right)^{\mathrm{m}} \\ \mathrm{W} = 1-\exp(-\mathrm{r}\bar{\varepsilon}) \\ \mathrm{r} = \mathrm{r}_0 + \mathrm{r}_1\mathrm{T} \\ \mathrm{r} = \mathrm{m}_0 + \mathrm{m}_1\mathrm{T} \end{cases} \tag{16}$$

The elastic strain rate tensor is given by the Hooke's relation :

$$\dot{\varepsilon}^{\mathrm{e}} = \frac{1+\upsilon}{\mathrm{E}}\dot{\sigma} - \frac{\upsilon}{\mathrm{E}}\mathrm{tr}(\dot{\sigma})\,\mathrm{Id} \tag{17}$$

and the normality rule is used to express the plastic strain rate tensor :

$$\begin{aligned} &\text{if } \mathrm{f}_{\mathrm{H}}(\sigma,\bar{\varepsilon},\dot{\bar{\varepsilon}},\mathrm{T}) < 0 \quad \dot{\varepsilon}^{\mathrm{p}} = 0 \\ &\text{if } \mathrm{f}_{\mathrm{H}}(\sigma,\bar{\varepsilon},\dot{\bar{\varepsilon}},\mathrm{T}) = 0 \begin{cases} \dot{\varepsilon}^{\mathrm{p}} = \dot{\lambda}^{\mathrm{p}} \dfrac{\partial \mathrm{f}(\sigma,\bar{\varepsilon},\dot{\bar{\varepsilon}},\mathrm{T})}{\partial\sigma} \\ \dot{\lambda}^{\mathrm{p}} \geq 0 \end{cases} \end{aligned} \tag{18}$$

One can notice that the plastic multiplier $\dot{\lambda}^{\mathrm{p}}$ is identified to the plastic strain rate $\dot{\bar{\varepsilon}}$.

2.3 FRICTION LAW

The simulations were performed using a Tresca friction law :

$$\tau = -\overline{\mathrm{m}}\sigma_0 \frac{\Delta \mathrm{v}_{\mathrm{t}}}{\sqrt{3}\left\|\Delta \mathrm{v}_{\mathrm{t}}\right\|} \tag{19}$$

where $\tau = \sigma\mathrm{n} - (\sigma\mathrm{n}.\mathrm{n})\mathrm{n}$ is the shear stress and $\Delta \mathrm{v}_{\mathrm{t}}$ the relative sliding velocity.

2.4 WEAK FORMULATION OF THE THERMO-MECHANICAL PROBLEM

The unilateral contact between the tool and the workpiece is treated using a penalty method :

$$\sigma \mathrm{n}.\mathrm{n} = \left\{ \begin{array}{cc} -\rho\left[(\mathrm{v}-\mathrm{v}_{\mathrm{die}}).\mathrm{n} - \dfrac{\mathrm{d}}{\Delta \mathrm{t}} \right] \text{if } (\mathrm{v}-\mathrm{v}_{\mathrm{die}}).\mathrm{n} \geq \dfrac{\mathrm{d}}{\Delta \mathrm{t}} \\ 0 \qquad\qquad \text{if } (\mathrm{v}-\mathrm{v}_{\mathrm{die}}).\mathrm{n} < \dfrac{\mathrm{d}}{\Delta \mathrm{t}} \end{array} \right\} \underset{\text{def}}{=} -\rho\left[(\mathrm{v}-\mathrm{v}_{\mathrm{die}}).\mathrm{n} - \frac{\mathrm{d}}{\Delta \mathrm{t}} \right]^{+} \text{ on } \partial\Omega_{\mathrm{c}} \quad (20)$$

where ρ is a penalty coefficient, d is the penetration distance between the die and the part, v is the velocity of the material point and $\mathrm{v}_{\mathrm{die}}$ the tool velocity.

Finally, in order to solve the thermo-mechanical problem using finite element methods, a weak formulation of problems (1), (2) and (3) is expressed as follows :

$$\left\{ \begin{array}{l} \text{find } (\mathrm{v},\mathrm{p}) \in \mathsf{V} \times \mathsf{P} \\ \displaystyle\int_{\Omega} \mathrm{s}(\mathrm{v}) : \dot{\varepsilon}^{*} \mathrm{d}\Omega - \int_{\Omega} \mathrm{p}.\mathrm{tr}(\dot{\varepsilon}^{*}) \mathrm{d}\Omega + \int_{\partial\Omega_{\mathrm{c}}} \rho\left[(\mathrm{v}-\mathrm{v}_{\mathrm{die}}).\mathrm{n} - \frac{\mathrm{d}}{\Delta \mathrm{t}} \right]^{+} \mathrm{v}^{*}.\mathrm{n} \ \mathrm{d}\Gamma - \int_{\partial\Omega_{\mathrm{c}}} \tau.\mathrm{v}^{*} \mathrm{d}\Gamma = 0 \quad \forall \mathrm{v}^{*} \in \mathsf{V} \quad (21) \\ \displaystyle\int_{\Omega} \mathrm{p}^{*}.\dot{\varepsilon}_{\mathrm{ii}} \mathrm{d}\Omega = -\int_{\Omega} \mathrm{p}^{*}.\frac{\dot{\mathrm{p}}}{\chi} \mathrm{d}\Omega \quad \forall \mathrm{p}^{*} \in \mathsf{P} \end{array} \right.$$

$$\text{find } \mathrm{T} \in \Theta \text{ such as}$$

$$\int_{\Omega} \rho \mathrm{c} \frac{\mathrm{dT}}{\mathrm{dt}} \mathrm{T}^{*} + \int_{\Omega} \mathrm{k} \nabla \mathrm{T}.\nabla \mathrm{T}^{*} = \int_{\Omega} \sigma : \dot{\varepsilon}^{\mathrm{p}} \mathrm{T}^{*} \quad \forall \mathrm{T}^{*} \in \Theta_{0} \qquad (22)$$

where Ω is the workpiece domain, V is the set of admissible velocities, P the set of admissible pressures, Θ the set of admissible temperatures satisfying $\mathrm{T} = \mathrm{T}_{\mathrm{int}}$ on $\partial\Omega_{\mathrm{c}}$, Θ_{0} the set of admissible temperatures satisfying $\mathrm{T} = 0$ on $\partial\Omega_{\mathrm{c}}$ and χ is the bulk modulus.

2.5 FINITE ELEMENT RESOLUTION

The mechanical problem is solved using a P1+/P1 mixed finite element method in velocity and pressure [6] and the thermal problem is solved using a P1 finite element method [7] on the same mesh. Indeed, the domain is discretised using a regular triangulation of Ω with tetrahedrons. The velocity, the pressure and the temperature are approximated by piecewise linear functions on Ω. Replacing v^{*}, p^{*} and T^{*} by basis vectors of the discretised functional

spaces, the discrete mechanical and thermal problems are written at time t_n as a discrete non linear system :

$$\begin{cases} R\left(\lambda, X^n, \bar{\varepsilon}^n, V^n, P^n, T^{n-1}\right) = 0 \\ C\dfrac{\Delta}{\Delta t}T^n + KT^n = Q\left(V^n\right) \end{cases} \tag{23}$$

where λ is the vector of parameters characterising the constitutive and/or the friction law, X^n is the vector of nodal coordinates of the mesh, $\bar{\varepsilon}^n$ is the computed equivalent plastic strain at time t_n and V^n, P^n, T^n are respectively the vectors containing the discrete velocity, hydrostatic pressure and temperature at time t_n.

As the mechanical problem is non linear with respect to V^n and P^n, it is solved using an iterative Newton-Raphson algorithm :

$$\begin{array}{l} \text{at time } t_n \\ j = 1 \\ \text{do while} \left\| \begin{pmatrix} V_j^n \\ P_j^n \end{pmatrix} \right\| \geq \varepsilon \ (\text{stop criterion}) \\ \quad \left| \begin{array}{l} \dfrac{\partial R_j^n}{\partial (V,P)} \begin{pmatrix} \Delta V_j \\ \Delta P_j \end{pmatrix} = -R_j^n \\ \begin{pmatrix} V_{j+1}^n \\ P_{j+1}^n \end{pmatrix} = \begin{pmatrix} V_j^n \\ P_j^n \end{pmatrix} + \beta \begin{pmatrix} \Delta V_j \\ \Delta P_j \end{pmatrix} \\ \\ j = j+1 \end{array} \right. \\ \left(V^n \ P^n\right)^T \leftarrow \left(V_j^n \ P_j^n\right)^T \end{array} \tag{24}$$

where $R\left(\lambda, X^n, \bar{\varepsilon}^n, V^n, P^n, T^{n-1}\right)$ is denoted R^n by sake of simplicity and β is a real number determined using a line search algorithm.

A forward Euler scheme is used to update the history variables :

$$X^{n+1} = X^n + \Delta t . V^n \tag{25}$$

and

$$\bar{\varepsilon}^{n+1} = \bar{\varepsilon}^{n} + \Delta t.\dot{\bar{\varepsilon}}^{n} \tag{26}$$

In this updated Lagrangian scheme, the nodes follow the material flow, so the mesh may degenerate during the simulation. In order to ensure a satisfying mesh quality, a remeshing algorithm is used [8].

3 FORMULATION OF THE INVERSE PROBLEM

3.1 STABILISED GAUSS-NEWTON ALGORITHM

The goal of the proposed inverse analysis is to identify some mechanical parameters using measurements provided by mechanical tests such as compression, torsion, bulging, etc… The inverse problem is expressed as a least square optimisation problem :

$$\begin{aligned} &\text{find } \lambda^{opt} \in \mathrm{IR}^{NPar} \text{ such as} \\ &\begin{cases} \phi\left(\lambda^{opt}\right) = \min\limits_{\left\{\lambda \in \mathrm{IR}^{NPar},\, \lambda_i^{min} < \lambda_i < \lambda_i^{max},\ i=1,..,NPar\right\}} \left(\phi(\lambda)\right) \\ \phi(\lambda) = \left(\mathrm{F}(\lambda) - \mathrm{M}\right)^{T} \mathrm{W}\left(\mathrm{F}(\lambda) - \mathrm{M}\right) \underset{def}{=} \left\|\mathrm{F}(\lambda) - \mathrm{M}\right\|_{\mathrm{W}}^{2} \end{cases} \end{aligned} \tag{27}$$

where λ is a vector containing the parameters to be identified, λ^{opt} is the optimal set of parameters, ϕ is the cost function, W is a diagonal weight matrix, F is the data computed by the direct model and M is a vector containing the experimental data.

Problem (27) is solved using a Gauss-Newton algorithm [9]:

$$\begin{aligned} &\text{do while}\left(\left\|\frac{d\phi}{d\lambda}\right\|_2 > \varepsilon_{stop}\right) \qquad (\text{stop criterion}) \\ &\begin{cases} \left(\dfrac{dF\left(\lambda^{n}\right)}{d\lambda}^{T} \mathrm{W} \dfrac{dF\left(\lambda^{n}\right)}{d\lambda}\right) d^{n} = -\dfrac{dF\left(\lambda^{n}\right)}{d\lambda}^{T} \mathrm{W}\left(\mathrm{F}\left(\lambda^{n}\right) - \mathrm{M}\right) \\ \lambda^{n+1} = \lambda^{n} + \beta_{ls} d^{n} \\ \\ n = n + 1 \end{cases} \end{aligned} \tag{28}$$

where d^n is the n^{th} Gauss-Newton step and β_{ls} is obtained using a line search algorithm. At each Gauss-Newton iteration, the determination of the step d^n may be seen as the resolution of the following optimisation sub-problem :

$$\begin{aligned} d^n &= \underset{d \in IR^{NPar}}{\operatorname{argmin}} \psi(d) \\ \psi(d) &= \frac{1}{2} d^T \left(\frac{dF(\lambda^n)}{d\lambda}^T W \frac{dF(\lambda^n)}{d\lambda} \right) d + d^T \frac{dF(\lambda^n)}{d\lambda}^T W\left(F(\lambda^n) - M\right) \end{aligned} \tag{29}$$

Finally, one can prove the following relation :

$$\left\| d^n \right\|_2 \leq \frac{1}{\alpha_{\min}} \left\| \frac{d\phi(\lambda^n)}{d\lambda^n} \right\|_2 . \tag{30}$$

where α_{min} is the lower the Gauss-Newton matrix eigenvalue. Hence, if the Gauss-Newton matrix is ill conditioned, the Gauss-Newton method may become unstable. When the modelling error is important (i.e. the final value of ϕ is relatively high) and the Gauss-Newton matrix is ill-conditioned, the step computed by the optimisation method may be important even though λ^n is close to the optimum. In order to penalise wide optimisation steps when the Gauss-Newton matrix is ill conditioned, sub-problem (29) is replaced by the following sub-problem :

$$\begin{aligned} d^n &= \underset{d \in IR^{NPar}}{\operatorname{argmin}} \psi(d) \\ \psi(d) &= \frac{1}{2} d^T \left(\frac{dF(\lambda^n)}{d\lambda}^T W \frac{dF(\lambda^n)}{d\lambda} \right) d + d^T \frac{dF(\lambda^n)}{d\lambda}^T W\left(F(\lambda^n) - M\right) + \alpha \|d\|_L^2 \\ \text{with } L_{ij} &= \frac{1}{\left|\lambda_i^{max} - \lambda_i^{min}\right|^2} \delta_{ij} \end{aligned} \tag{31}$$

The solution of the above sub-problem satisfies the following inequality (c.f. Appendix) :

$$\left\| d^n \right\|_L \leq \frac{1}{\left|\alpha_i^R + \alpha\right|} \left\| \frac{d\phi(\lambda^n)}{d\lambda^n} \right\|_{L^{-1}} \tag{32}$$

where α_{min}^{R} is the lower eigenvalue of the matrix H defined as following :

$$\begin{aligned} H &= R^{-1}\frac{dF(\lambda^n)}{d\lambda}^T W \frac{dF(\lambda^n)}{d\lambda} R^{-1} \\ \text{with } R_{ij} &= \frac{1}{\left|\lambda_i^{max} - \lambda_i^{min}\right|}\delta_{ij} \end{aligned} \tag{33}$$

From relation (32), one can deduce :

$$\left\|d^n\right\|_L \leq \frac{1}{\alpha}\left\|\frac{d\phi(\lambda^n)}{d\lambda^n}\right\|_{L^{-1}} \tag{34}$$

If we want to impose $\left\|d^n\right\|_L \leq \sqrt{NPar}$, the following relation comes :

$$\alpha = \frac{1}{\sqrt{NPar}}\left\|\frac{d\phi(\lambda^n)}{d\lambda^n}\right\|_{L^{-1}} = \sqrt{\frac{\sum_{i=1}^{NPar}\left(\left(\frac{d\phi(\lambda^n)}{d\lambda^n}\right)_i\left(\lambda_i^{max} - \lambda_i^{min}\right)\right)^2}{NPar}} \tag{35}$$

One can notice that the stabilisation coefficient α tends to zero when the gradient of the cost function vanishes. This methods aims at determining automatically a stabilisation parameter which avoids the determination of wide Gauss-Newton steps in comparison with the parameter variation range. Within this framework, the lower eigenvalues may be filtered if it is necessary.

3.2 STABILITY ANALYSIS

Once the optimal set of parameters is obtained, it may be interesting to study the stability of the inverse analysis. The computation of the sensitivity matrix allows to study the stability of the developed inverse module [12]. The stability analysis consists in studying the influence of an experimental data perturbation on the optimal set of parameters. The optimal set of parameters is defined by the following relation :

$$\frac{d\phi(\lambda)}{d\lambda} = 2\frac{dF(\lambda)^T}{d\lambda}W(F(\lambda) - M) = 0 \tag{36}$$

If the experimental data M is replaced by a perturbed experimental data M+δM, one can denote the perturbed optimal set of parameters λ+δλ and the following relation holds :

$$2\frac{\mathrm{dF}(\lambda)^{\mathrm{T}}}{\mathrm{d}\lambda}\mathrm{W}\left(\mathrm{F}(\lambda)+\frac{\mathrm{dF}(\lambda)}{\mathrm{d}\lambda}\delta\lambda-\mathrm{M}-\delta\mathrm{M}\right)\approx 0 \tag{37}$$

Finally, one can prove that :

$$\begin{aligned}&\left|\delta\lambda_{\mathrm{k}}\right|\le\sqrt{\mathrm{G}_{\mathrm{kk}}}.\left\|\delta\mathrm{M}\right\|_{\mathrm{W}}\\&\text{where}\,\mathrm{G}=\left(\frac{\mathrm{dF}(\lambda)^{\mathrm{T}}}{\mathrm{d}\lambda}\mathrm{W}\frac{\mathrm{dF}(\lambda)}{\mathrm{d}\lambda}\right)^{-1}\end{aligned} \tag{38}$$

One can notice that this analysis is based on a first order approximation and that the inequality holds only for small perturbations. Finally, the stability analysis is able to indicate whether a parameter can be identified accurately or not.

Some parameters may be determined with an important uncertainty because of a lack of sensitivity of the measurements. This means that the experiments are not adequate to determinate these parameters. Uncertainty on the parameters may also be caused by important correlation effects between some parameters. If some parameters are highly correlated, the cost function shows a valley close to the optimum. Therefore, the columns of the sensitivity matrix are not linearly independent and the Gauss-Newton matrix degenerates [13]. The cross effects between pairs of parameters can be detected by using some appropriate indicators. Let us define the cosinus between two sensitivities as follow :

$$\underset{\mathrm{W}}{\cos}\left(\frac{\mathrm{dF}}{\mathrm{d}\lambda_{\mathrm{i}}},\frac{\mathrm{dF}}{\mathrm{d}\lambda_{\mathrm{j}}}\right)=\frac{\left(\frac{\mathrm{dF}}{\mathrm{d}\lambda_{\mathrm{i}}},\frac{\mathrm{dF}}{\mathrm{d}\lambda_{\mathrm{j}}}\right)_{\mathrm{W}}}{\left\|\frac{\mathrm{dF}}{\mathrm{d}\lambda_{\mathrm{i}}}\right\|_{\mathrm{W}}\left\|\frac{\mathrm{dF}}{\mathrm{d}\lambda_{\mathrm{j}}}\right\|_{\mathrm{W}}} \tag{39}$$

where $\left(\frac{\mathrm{dF}}{\mathrm{d}\lambda_{\mathrm{i}}},\frac{\mathrm{dF}}{\mathrm{d}\lambda_{\mathrm{j}}}\right)_{\mathrm{W}}=\frac{\mathrm{dF}}{\mathrm{d}\lambda_{\mathrm{i}}}^{\mathrm{T}}\mathrm{W}\frac{\mathrm{dF}}{\mathrm{d}\lambda_{\mathrm{j}}}$

Then, if $\left| \underset{w}{\cos}\left(\frac{dF}{d\lambda_i}, \frac{dF}{d\lambda_j} \right) \right|$ is close to 1, the Gauss-Newton matrix is ill-conditioned and it is difficult to discriminate the effects of the parameters on the measurements.

4 SENSIVITY ANALYSIS

The sensitivity analysis is a necessary step to compute first order optimisation methods and for the stability analysis. The finite difference method [10] is the most simple algorithm because it uses the direct model as a black box. In counterpart, this method is relatively slow and its accuracy depends on the discretisation step. Many authors prefer to use an analytical sensitivity analysis (see [1], [3] and [11]). This method is very precise and linear, but its development requires many calculations when the direct model is complex. In this work we have chosen to use a semi-analytical scheme, which combines certain advantages of the analytical and of the finite difference methods. The semi-analytical method [4],[2] is based on a first order approximation of the derivative of F with respect to λ :

$$\frac{dF}{d\lambda} = \frac{F\left(\lambda + \Delta\lambda, V + \Delta\lambda \frac{dV}{d\lambda}, P + \Delta\lambda \frac{dP}{d\lambda}, T + \Delta\lambda \frac{dT}{d\lambda} \right) - F(\lambda, V, P, T)}{\Delta\lambda} + O(\Delta\lambda) \qquad (40)$$

where $\Delta\lambda$ is the finite difference step. The derivatives of the velocity, of the pressure and of the temperature with respect to the parameters to be identified are obtained from the differentiation of system (23) :

$$\frac{\partial R}{\partial(V, P)} \begin{pmatrix} \frac{dV}{d\lambda} \\ \frac{dP}{d\lambda} \end{pmatrix} = -\left. \frac{dR}{d\lambda} \right|_{(V,P)\text{fixed}} \qquad (41)$$

$$C \frac{\Delta}{\Delta t} \left(\frac{dT}{d\lambda} \right) + K \left(\frac{dT}{d\lambda} \right) = \frac{dQ(V)}{d\lambda} \qquad (42)$$

One should stress that the tangent systems are linear, contrary to those of the direct model. The matrices involved in linear systems (41) and (42) are already evaluated in the direct model for solving the thermo-mechanical problem (23). Then, it is only necessary to compute

the right hand sides of linear systems (41) and (42). In order to avoid the calculation of the right hand sides, a first order finite difference scheme can be used :

$$\frac{\partial R}{\partial (V,P)}\begin{pmatrix}\frac{dV}{d\lambda}\\ \frac{dP}{d\lambda}\end{pmatrix} \approx -\frac{R^p - R}{\Delta\lambda} \tag{43}$$

and

$$C\frac{d}{dt}\left(\frac{dT}{d\lambda}\right)+K\left(\frac{dT}{d\lambda}\right)\approx \frac{Q\left(V+\Delta\lambda\frac{dV}{d\lambda}\right)-Q(V)}{\Delta\lambda} \tag{44}$$

with

$$R^p = R\left(\lambda+\Delta\lambda, X^n+\Delta\lambda.\frac{dX^n}{d\lambda}, \bar{\varepsilon}^n+\Delta\lambda.\frac{d\bar{\varepsilon}^n}{d\lambda}, V^n, P^n, T^{n-1}+\Delta\lambda.\frac{dT^{n-1}}{d\lambda}\right) \tag{45}$$

and

$$R = R\left(\lambda, X^n, \bar{\varepsilon}^n, V^n, P^n, T^{n-1}\right) \tag{46}$$

The derivatives of the history variables are then updated :

$$\frac{dX^{n+1}}{d\lambda} = \frac{dX^n}{d\lambda} + \Delta t.\frac{dV^n}{d\lambda} \tag{47}$$

and

$$\frac{d\bar{\varepsilon}^{n+1}}{d\lambda} = \frac{d\bar{\varepsilon}^n}{d\lambda} + \Delta t.\frac{d\dot{\bar{\varepsilon}}^n}{d\lambda} \tag{48}$$

Finally, this scheme gathers some advantages of the analytical scheme and of the finite difference scheme. Indeed, the semi-analytical sensitivity analysis is linear and is relatively simple to compute because of the local finite difference schemes. Moreover, the sensitivity analysis module is easily updated when the direct model is modified. This method allows to study different mechanical tests in order to characterise different constitutive laws.

5 APPLICATIONS

5.1 PLANE STRAIN COMPRESSION TEST

The inverse analysis described in this paper has been applied to the analysis of the plane strain compression test. During this test, parallelepiped brass samples are upset between two dies (Figure 1).

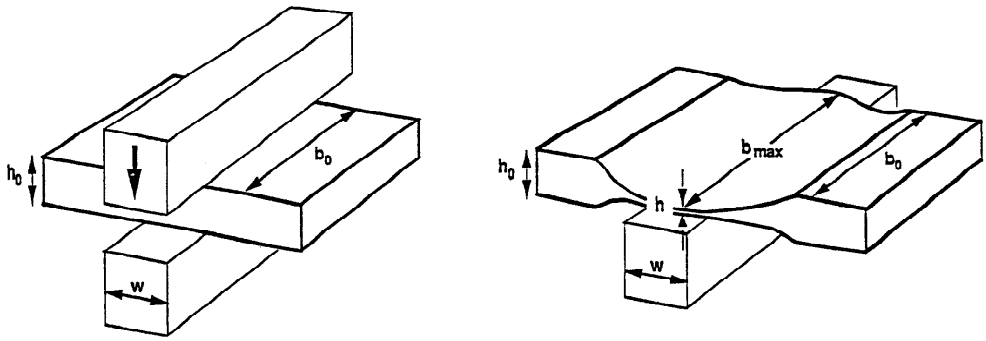

Figure 1: Plane strain compression test

The strain state generated in this mechanical test is relatively close to the strain state encountered during the rolling process. Then, it is generally used to characterise materials to be formed using a rolling process. As the material is deformed, the time versus load curves are recorded. The influence of the constitutive and of the friction coefficients on the load may be difficult to discriminate. In order to decouple the effects of the friction and of the constitutive coefficients on the load, two different sample heights are used.

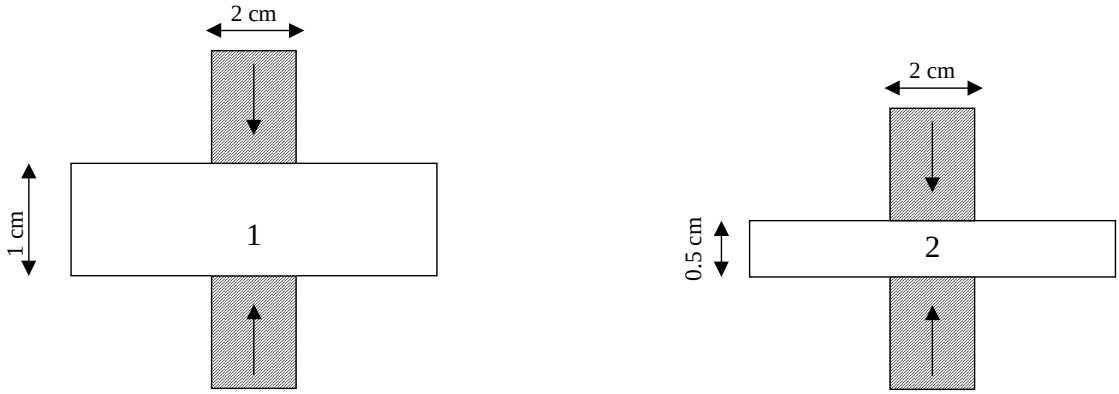

Figure 2: Sample dimensions

The material behaviour is modeled using the Von Mises plasticity criterion and the flow stress (16). The tools are piloted using an average strain rate definied as follows :

$$\dot{\bar{\varepsilon}}_{av} = \frac{V_{die}}{h} \qquad (49)$$

where v_{die} is the die velocity and h the sample height. An experimental plan (TAB 1) is used to provide enough data for ensuring the identifiability condition [14].

Temperatures $\dot{\bar{\varepsilon}}_{av}$		550	600	650	700
0.1	geometry 1	+		+	+
	geometry 2	+		+	+
5	geometry 1	+	+		+
	geometry 2		+		+

TAB 1: Experimental plan

The constitutive coefficients of model (16) and the friction coefficient of the Tresca law are identified using the developped inverse model. The result of the identification process is show in TAB 2.

$\overline{m}$	0.53
K_0 (KPa.s^m)	152
m_0	-0.13
m_1(K^{-1})	$4.59.10^{-4}$
n	0.1
β (K)	4915
r_0	0.96
r_1(K^{-1})	$2.49.10^{-3}$
K_{sat} (KPa.s^m)	9.8
β_{sat} (K)	6636
ϕ_{final}	10.9%

TAB 2: results of the estimation

A total of 14 iterations were necessary to reach the optimal set of parameters. One notices that the Gauss-Newton method does not convergence if the stabilisation method is not used. Figures 3 to 6 show a good agreement between computed and experimental loads.

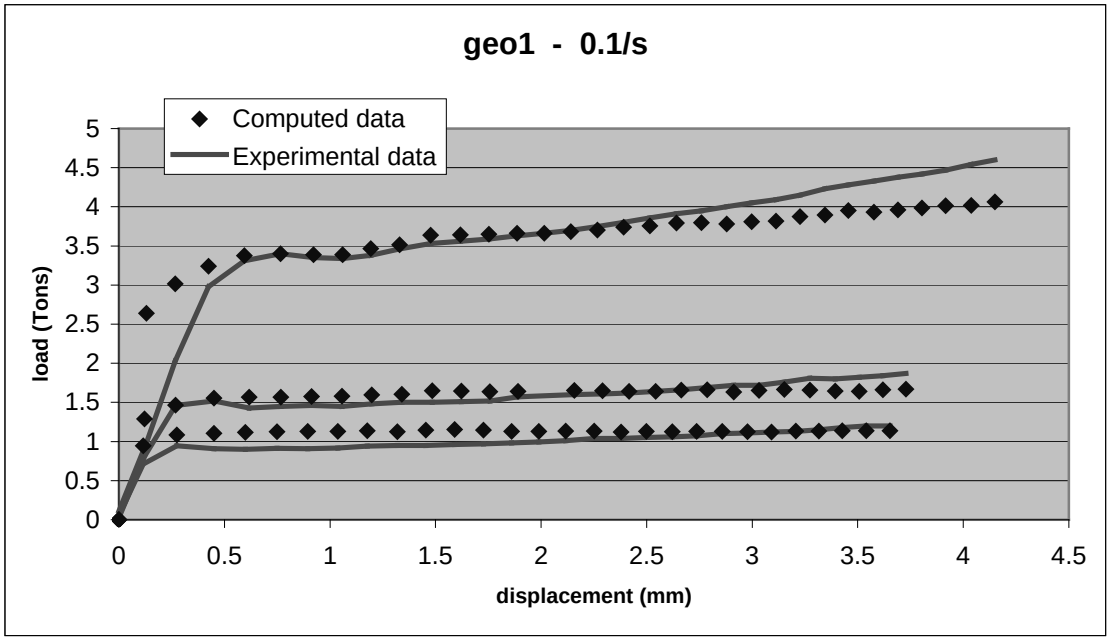

Figure 3 : Comparison between the computed and the experimental load for the first geometry and for an average strain rate at 0.1/s

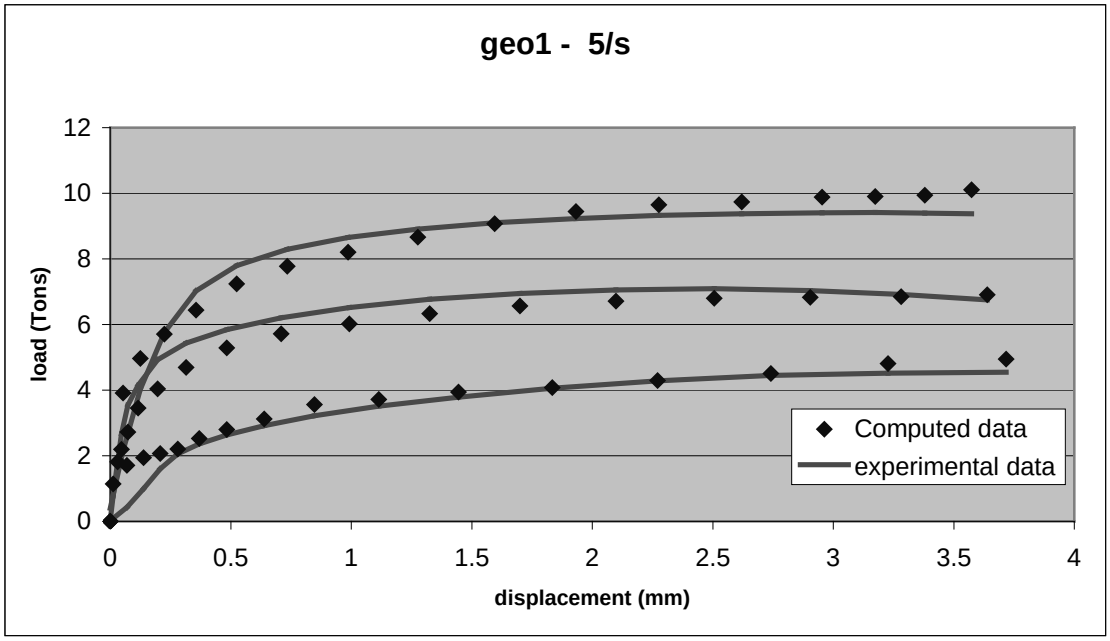

Figure 4 : Comparison between the computed and the experimental load for the first geometry and for an average strain rate at 5/s

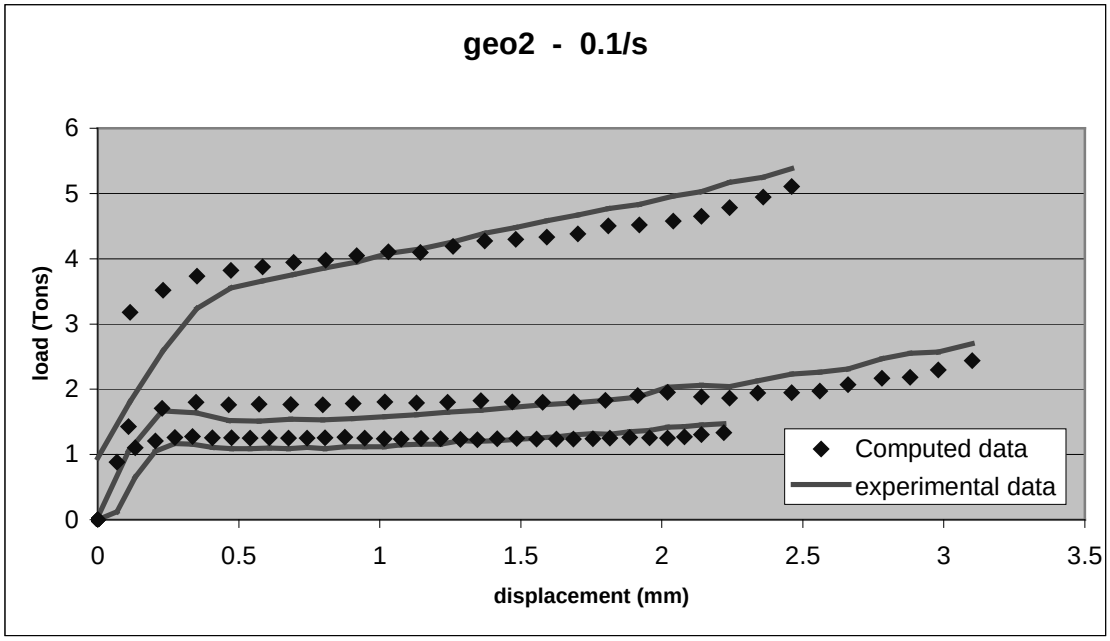

Figure 5 : Comparison between the computed and the experimental load for the second geometry and for an average strain rate at 0.1/s

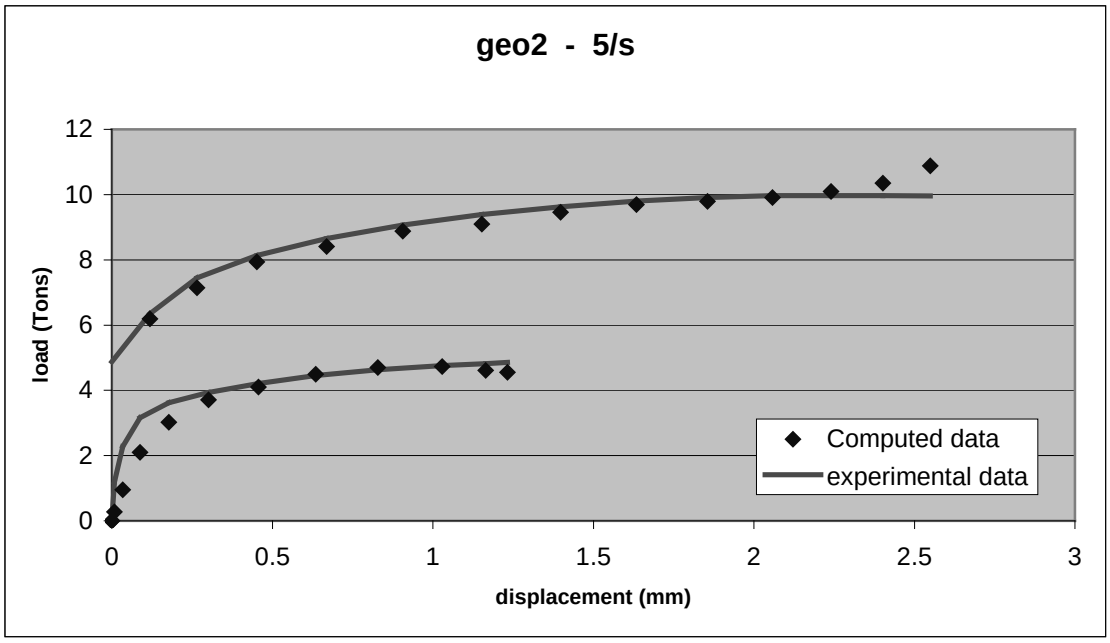

Figure 6 : Comparison between the computed and the experimental load for the second geometry and for an average strain rate at 5/s

5.2 BULGE TEST

5.2.1 DESCRIPTION OF THE EXPERIMENT

Circular samples cut out of steel sheets are clamped using a circular blank holder. The samples are bulged thanks to a pressured fluid. Sequences of images are taken with two CCD cameras during bulging and they are compared to an initial reference image using ARAMIS, a pattern recognition system [15] (see Figure 7).

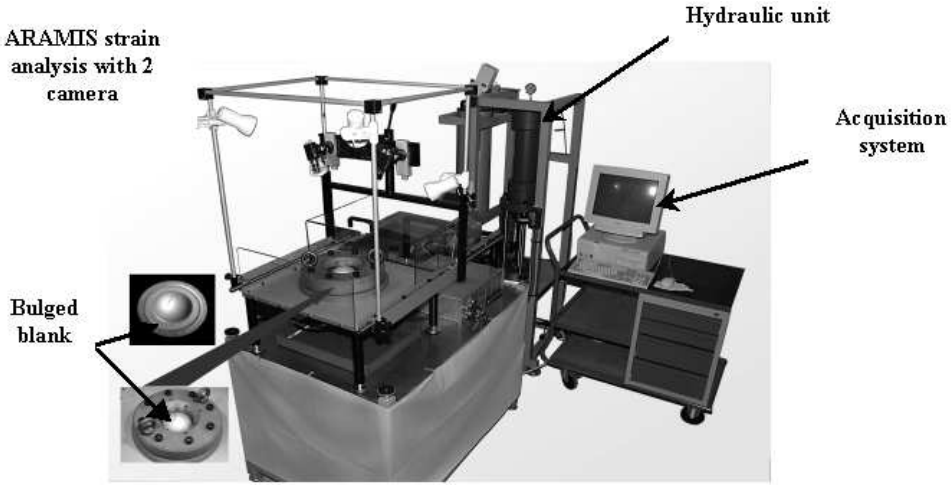

Figure 7 : Bulging machine

The evolution of strain field with respect to time is deduced from this analysis.

5.2.2 INVERSE ANALYSIS OF THE CIRCULAR BULGING TEST

The inverse module previously presented is used to find out constitutive parameters of the steel from sheet shape measurements. The Von Mises yield criterion (11) and the constitutive law (15) are used to model the behaviour of the material. The evolution of the positions of five points on the sheet is used for the parameter identification. An axisymetric software FORGE2® is able to simulate the bulge test. Within this framework, the cost function is written as follows :

$$\phi(\lambda) = \sum_{j=1}^{j=NbPoint} \frac{\sum_{i=1}^{i=Ni} \left\| X_j^{cal}(t_i) - X_j^{exp}(t_i) \right\|^2}{\sum_{i=1}^{i=Ni} \left\| X_j^{exp}(t_i) \right\|^2} \qquad (50)$$

where NbPoint is the number of points used for the identification (i.e. 5), Ni is the number of images used, $X_j^{cal}(t_i)$ is the position of the j-th point computed by FORGE2® and $X_j^{exp}(t_i)$ is the position of the j-th measured point at time t_i. Two Gauss-Newton iterations are necessary to reach the optimal set of parameters. The identified parameters are K=518 KPa.s and n= 0.206, and the final cost function value is 2.6%. A very good agreement between computed and experimental shape is shown at the end of the identification (see Figure 8).

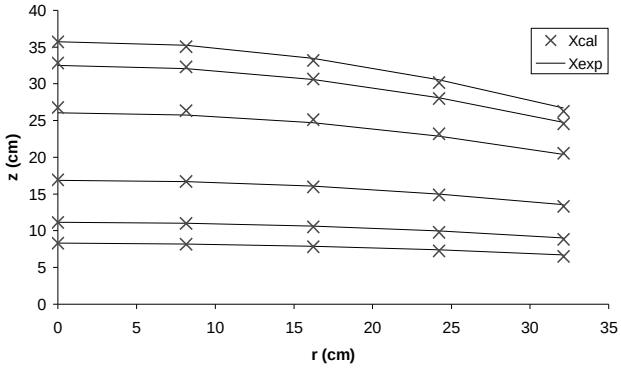

Figure 8 : Evolution of the shape of the sample with respect to the time, X=(r,z)

Therefore, the stability analysis shows that the parameters are well defined by the data:

$$\frac{|\delta K|}{|K|} \le 3.6 \frac{\|\delta X\|_2}{\|X\|_2}$$
$$\frac{|\delta n|}{|n|} \le 9.0 \frac{\|\delta X\|_2}{\|X\|_2} \qquad (51)$$

This result indicates that, even though the evolution of the shape is well reproduced by FORGE2®, it is necessary to use accurate experimental data to determine the value of n. Finally, this example shows that the bulge tests can be studied using an inverse method. The main advantage of this approach is that no analytical model of the bulge test has to be used. Moreover, the stability analysis provides an information about the quality of the results given by the inverse model.

5.2.3 INVERSE ANALYSIS OF THE ELLIPTIC BULGING TEST

The behaviour of a metallic sheet have been modelled using the Hill'48 yield criterion (13)-(14) and the flow stress (15). In this section, the bulging tests are performed using an elliptic blank in order to find out the Hill criterion and flow stress parameters. In order to validate the

method, artificial experimental data is used for the inverse analysis, generated with FORGE3®, using the following set of parameters.

F	0.4
G	0.5
H	0.6
K (MPa)	0.54
n	0.15

TAB 3 : Nominal values of the constitutive parameters

At least two experiments are necessary to characterise the material. The main axis of the elliptic blank is aligned with the rolling direction in the first experiment, and is perpendicular to the rolling direction in the second experiment. The goal is to identify F, H, K_0 and n from the displacement measurements of three points (denoted A, B and C) on the surface of the sheet.

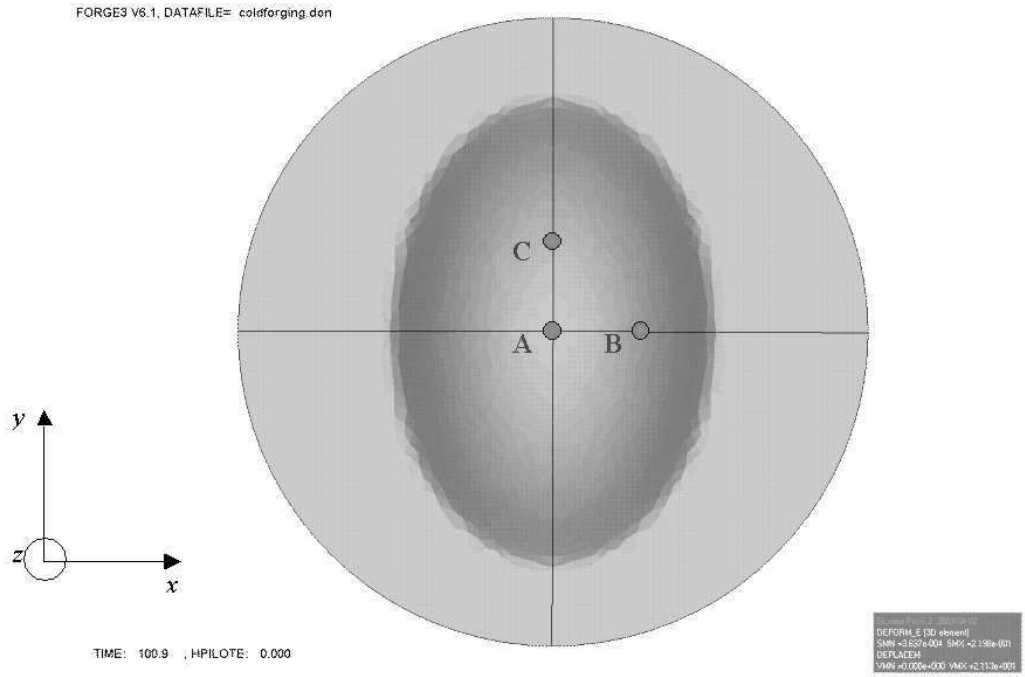

Figure 9 : Measurement point locations

Seven Gauss-Newton iterations are necessary to converge and the results of the identification are shown in Figures 6 to 8. A good agreement between computed and experimental data is obtained and the final cost function value is close to 0.1%.

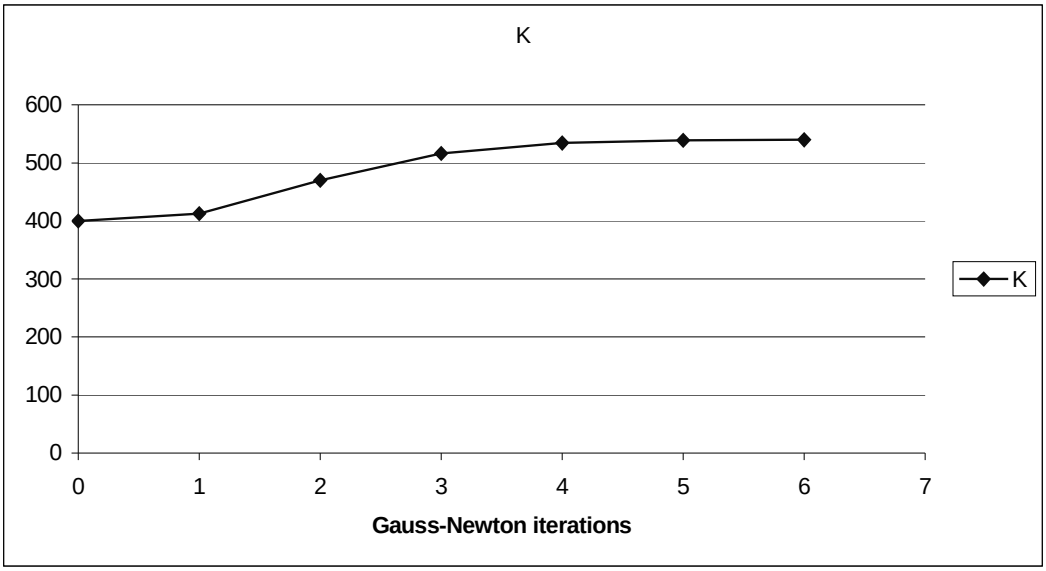

Figure 10 : Evolution of K with respect to Gauss-Newton iterations

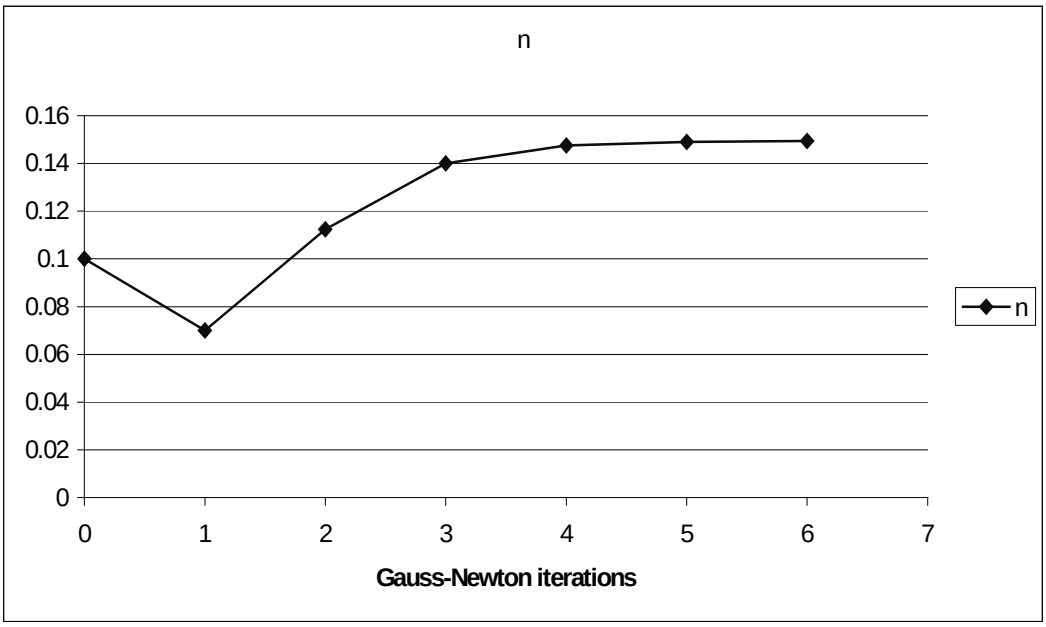

Figure 11 : Evolution of n with respect to Gauss-Newton iterations

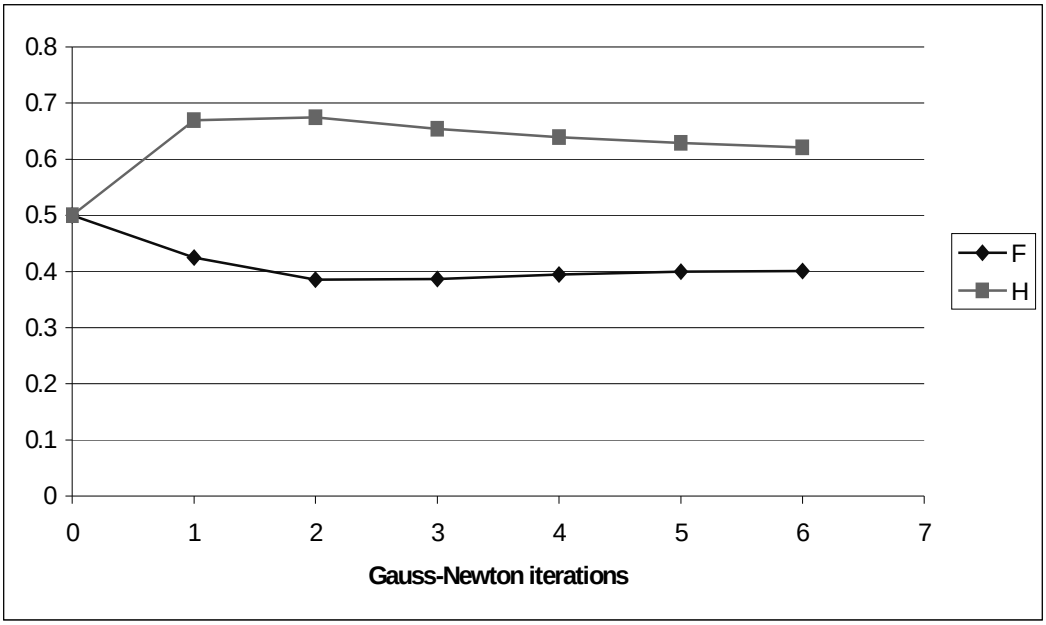

Figure 12 : Evolution of F and H with respect to Gauss-Newton iterations

The L, M and N parameters cannot be identified because there is no shearing during the bulging tests. Indeed, there is no influence of these parameters on the shape of the sheet. The parameter values at the end of the identification process are the following :

F	0.4006
G	0.5
H	0.62
K_0 (MPa)	0.539
n	0.149

6 CONCLUSION

An inverse method coupled to a 3D FEM direct model is presented in this work. The semi-analytical sensitivity analysis allows to identify various constitutive law parameters without any adaptation of the inverse module. Moreover, the direct model, FORGE3® is able to model different mechanical tests. Therefore, the inverse method presented in this paper allows to identify various constitutive parameters using various mechanical tests.

The proposed stabilised inverse method provides satisfying results on various test cases. The identification of ten parameters of a constitutive and of a friction law have been done from a

PSC test. The proposed approach has also been used to analyse the bulging test : circular bulging tests can be used to find out the constitutive parameters of a metallic sheet, and elliptic bulging tests can provide Hill's anisotropic coefficients.

REFERENCES

1. A. Gavrus, E. Massoni, J.L. Chenot, An inverse analysis using a finite element model for identification of rheological parameters, Journal of materials processing technology, 60 (1996) 447-454.

2. E. Massoni, B. Boyer, R. Forestier, Inverse analysis of thermomechanical upsetting tests using gradient method with semi-analytical derivatives, International journal of thermal sciences, 41 (2002) 557-563.

3. R. Mahnken, E. Stein, A unified approach for parameter identification of inelastic material models in the frame of the finite element method, Computer methods in applied mechanics and engineering, 136 (1996) 225-258.

4. E. S. Jochen, D. A. Tortorelli, Inverse heat conduction problem solutions via second-order design sensitivities and Newton's method, Inverse Problems in Engineering, Vol. 2 (1995) 227-262.

5. R. Hill, A theory of the yielding and of plastic flow of anisotropic metals, Proceedings of the Royal Society of London, Serie A, 193 (1948) 281-397.

6. M. Fortin, D.N. Arnold, F. Brezzi, A stable finite element for the Stokes equations. Calcolo, 21 (1984) 337 344.

7. C. Aliaga, E. Massoni, J.L. Treuil, 3D numerical simulation of THEVP behavior using stabilized mixed F.E. formulation: application to 3D heat treatment, Proceedings of the Fourth World Congress on Computational Mechanics, Buenos Aires, Argentina, 29th of June, 2nd of July 1998.

8. T. Coupez, Grandes déformations incompressibles-remaillage automatique. PhD thesis, ENSMP, France,1991.

9. J.F. Bonnans, J.C. Gilbert, C. Lemaréchal, C. Sagastizàbal, Optimisation Numérique, Springer, 1997.

10. D.S. Schnur, N. Zabaras, An inverse method for determining elastic material properties and a material interface, 33 (1992) 2039-2057.

11. J.C. Gelin, O. Ghouati, An inverse solution procedure for material parameters identification in large plastic deformation, Communications in numerical methods in engineering, 12 (1996) 161-173.

12. B. F. Blackwell, K. J. Downing, Sensitivity and uncertain analysis for thermal problems, Proceedings of the 4th International Conference on Inverse Problems in Engineering: Theory and Practice, Rio de Janeiro, 26th –31st of may 2002.

13. R. Forestier, Y. Chastel, E. Massoni, 3D inverse analysis model using semi-analytical differentiation for mechanical parameter estimation, Proceedings of the 4th International Conference on Inverse Problems in Engineering, Rio de Janeiro, 2002.

14. J. V. Beck, K. V. Arnold, Parameter estimation in engineering and science, New York, Wiley ,1977.

15. http://www.gom.com/

APPENDIX

The stabilised Gauss Newton step is given by the following relationship :

$$\left(\frac{\mathrm{dF}\left(\lambda^{\mathrm{n}}\right)}{\mathrm{d}\lambda}^{\mathrm{T}} \mathrm{W} \frac{\mathrm{dF}\left(\lambda^{\mathrm{n}}\right)}{\mathrm{d}\lambda} + \alpha \mathrm{RR} \right) \mathrm{d}^{\mathrm{n}} = - \frac{\mathrm{d}\phi\left(\lambda^{\mathrm{n}}\right)}{\mathrm{d}\lambda} \tag{52}$$

$$\mathrm{R}_{\mathrm{ij}} = \frac{1}{\left| \lambda_{\mathrm{i}}^{\max} - \lambda_{\mathrm{i}}^{\min} \right|} \delta_{\mathrm{ij}} \tag{53}$$

where α is the stabilisation parameter and δ_{ij} is the Kronecker delta.

From (52), one can deduce that :

$$\left(\mathrm{R}^{-1} \frac{\mathrm{dF}\left(\lambda^{\mathrm{n}}\right)}{\mathrm{d}\lambda}^{\mathrm{T}} \mathrm{W} \frac{\mathrm{dF}\left(\lambda^{\mathrm{n}}\right)}{\mathrm{d}\lambda} \mathrm{R}^{-1} + \alpha \mathrm{I} \right) \mathrm{R}\, \mathrm{d}^{\mathrm{n}} = -\mathrm{R}^{-1} \frac{\mathrm{d}\phi\left(\lambda^{\mathrm{n}}\right)}{\mathrm{d}\lambda} \tag{54}$$

One can obtain the following inequality :

$$\left\| \mathrm{R} \mathrm{d}^{\mathrm{n}} \right\|_2^2 \leq \frac{1}{\left(\alpha + \alpha_{\mathrm{i}}^{\mathrm{R}}\right)^2} \left\| \mathrm{R}^{-1} \frac{\mathrm{d}\phi\left(\lambda^{\mathrm{n}}\right)}{\mathrm{d}\lambda} \right\|_2^2 \tag{55}$$

where $\alpha_{\min}^{\mathrm{R}}$ is the smallest eigenvalue of the matrix H defined as :

$$H = \left(R^{-1} \frac{dF(\lambda^n)}{d\lambda}^T W \frac{dF(\lambda^n)}{d\lambda} R^{-1} \right) \tag{56}$$

Finally, if we denote L the matrix defined as :

$$L = RR \tag{57}$$

then

$$\left\| d^n \right\|_L^2 \leq \frac{1}{(\alpha + \alpha_i^R)^2} \left\| \frac{d\phi(\lambda^n)}{d\lambda} \right\|_{L^{-1}}^2 \tag{58}$$